Equilibrium Properties of Spherical Torus Plasmas in NSTX*

S. A. Sabbagh[1], S. M. Kaye[2], J. Menard[2], F. Paoletti[1], M. Bell[2], R. E. Bell[2], J. Bialek[1], M. Bitter[2], E. Fredrickson[2], D. Gates[2], A. H. Glasser[5], H. Kugel[2], L. L. Lao[3], B. LeBlanc[2], R. Maingi[4], R. Maqueda[5], E. Mazzucato[2], D. Mueller[2], M. Ono[2], S. Paul[2], M. Peng[4], C. Skinner[2], D. Stutman[6], G. A. Wurden[5], W. Zhu[1], and the NSTX Research Team

[1]Department of Applied Physics and Applied Mathematics, Columbia University, New York, NY, USA (sabbagh@pppl.gov)
[2]Princeton Plasma Physics Laboratory, Princeton University, Princeton, NJ, USA
[3]General Atomics, San Diego, CA, USA
[4]Oak Ridge National Laboratory, Oak Ridge, TN, USA
[5]Los Alamos National Laboratory, Los Alamos, NM, USA
[6]Johns Hopkins University, Baltimore, MD, USA

Abstract. Research in the National Spherical Torus Experiment, NSTX, has been conducted to establish spherical torus plasmas to be used for high-β, auxiliary heated experiments. The device has a major radius R_0 = 0.86 m, a midplane half-width of 0.7 m, and has been operated with toroidal magnetic field $B_0 \leq 0.3$ T and $I_p \leq 1.0$ MA. The evolution of the plasma equilibrium is analyzed between shots with an automated version of the EFIT code. Limiter, double-null, and lower single-null diverted configurations have been sustained for several energy confinement times. Plasma stored energy has reached 92 kJ (β_t = 17.8 %) with neutral beam heating. Plasma elongation of $1.6 \leq \kappa \leq 2.0$ and triangularity in the range $0.25 \leq \delta \leq 0.45$ have been sustained, with values of $\kappa = 2.5$ and $\delta = 0.6$ being reached transiently. The reconstructed magnetic signals are fit to the corresponding measured values with low error. Aspects of the plasma boundary, pressure, and safety factor profiles are supported by measurements from non-magnetic diagnostics. Plasma densities have reached 0.8 and 1.2 times the Greenwald limit in deuterium and helium plasmas, respectively, with no clear limit encountered. Instabilities including sawteeth and reconnection events (REs), characterized by Mirnov oscillations, and perturbation of the l_i, κ, and ℓ_i evolution, have been observed. A low q limit was observed and is imposed by a low toroidal mode number kink instability.

1. Introduction

The spherical torus (ST), a very low aspect ratio variant of the standard tokamak, offers potential advantages as a fusion energy reactor [1]. The most attractive ST reactor designs have both high fusion power and high bootstrap current fraction. To achieve this operation, both high toroidal β, $\beta_t \equiv 2\mu_0 \langle p \rangle / B_0^2$, and high normalized β, $\beta_N \equiv 10^8 \langle \beta_t \rangle a B_0 / I_p$ are required. Stable, experimental high $\beta_N < 6$ ST equilibria have been demonstrated in the START [2] device. The promising results obtained in this relatively small scale machine (plasma current, $I_p \leq 0.3$ MA) have encouraged the recent construction and initial operation of larger ST devices such as MAST [3] and the National Spherical Torus Experiment (NSTX) [4]. These machines are capable of operating with increased plasma current of 1 MA or greater. Auxiliary heating power systems for NSTX are designed to exceed 10 MW.

In any new device, a primary goal is to establish reproducible plasma configurations required for future experimentation. A basic and essential component of the analysis of these configurations is the accurate reconstruction of free-boundary magnetohydrodynamic (MHD) equilibria based on experimental measurements. The techniques used to reconstruct NSTX equilibria are described in Section 2. The experimental production of the main equilibrium configurations envisioned during the design phase of NSTX along with the response of the equilibrium to observed plasma phenomena is discussed in Section 3. Observed instabilities and operational limits are also discussed in this section. Ideal MHD stability limits for NSTX are discussed in Section 4.

2. Equilibrium reconstruction technique

Free-boundary plasma equilibrium reconstructions were obtained by utilizing the EFIT algorithm, full details of which can be found in Ref. [5]. The technique is summarized below, followed by specific additions and constraints required to model the NSTX configuration.

2.1. General technique

The free-boundary equilibrium is computed by satisfying MHD force balance through solution of the Grad-Shafranov equation

$$R^2 \nabla\bullet(\nabla\psi / R^2) = - R J_t \quad (1)$$

in the plasma (inner) region, and matching measured poloidal fluxes, magnetic fields, and imposed currents in the force-free (outer) region. Here, R is the cylindrical radial coordinate, and J_t is the toroidal current density in the plasma. The poloidal flux stream function, ψ, in the entire rectangular computational domain is obtained through a Picard iteration technique in which ψ is advanced by

$$\psi^{(m+1)}(r) = \Sigma\, G(r,r) I_c + \int_{v(m)} dR'dZ'\; G(r,r')\, J_t(R', \psi^{(m)}) \quad (2)$$

while iteratively minimizing the difference between measured and computed values in a least-squared sense

$$\chi^2 = \Sigma\, ((M_i - C_i)/\sigma_i)^2 \quad (3)$$

where M_i is a measured value or other constraint, C_i is the computed analog, and σ_i is the error associated with the measurement or constraint. Here, I_c are the imposed currents in external coils and conductors, and $G(r,r')$ is the toroidal Green function. The Green function is typically computed once for a given modeled system, and stored in tabular form for subsequent processing. The toroidal plasma current

$$\mu_0 J_t = \mu_0 R\, p'(\psi) + ff'(\psi) / R \quad (4)$$

is defined by the two flux functions p' and ff', which are the plasma pressure gradient and poloidal current functions, with $f = RB_t$. In general, two such flux functions are arbitrary, and an equilibrium solution requires that these two functions be defined. A set of basis functions is used to specify p' and ff', with a set of free parameters used to allow the self-consistent solution of the equilibrium constraint and simultaneous minimization of χ^2. As in Ref. [5], a general set of polynomial basis functions is chosen of the form

$$p'(\psi) = \Sigma\, A_i\, \psi_n^{\,i} \quad (5)$$

$$ff'(\psi) = \Sigma\, B_i\, \psi_n^{\,i} \quad (6)$$

where ψ_n is the poloidal flux normalized to the poloidal flux between the plasma boundary and the magnetic axis. The specific choice of polynomial order and constraint of these functions for NSTX equilibria is discussed in Section 2.2.

2.2. Specific considerations for spherical tori and NSTX implementation

EFIT has been applied to many tokamaks, including DIII-D, JET, and JT-60U. Each implementation has specific aspects required to properly model the particular configuration. NSTX reconstructions typically utilize data from more than 70 magnetic diagnostics including as many as 9 currents in the shaping and ohmic heating coils, 42 magnetic flux loops, 9 loop voltage monitors, 16 integrated local dB/dt pickup coils, and a Rogowski coil measuring the total toroidal current in the plasma, vacuum vessel, copper stabilizer plates, and lower divertor coil. The poloidal cross-section of the NSTX device, illustrating the diagnostics and conducting structure are shown in FIG. 1.

Special aspects of the NSTX EFIT implementation are primarily due to the low aspect ratio of a spherical torus. In particular, the inclusion of a sufficiently detailed model of the conducting

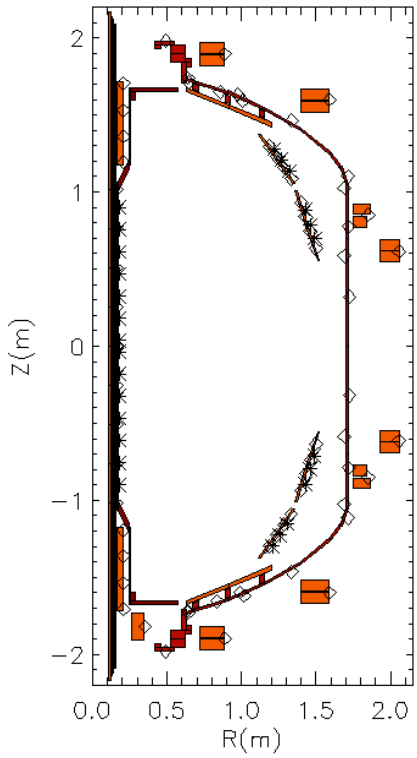

FIG. 1. Magnetic field coils, conducting structure, and magnetic diagnostics of NSTX. Open diamonds represent toroidal flux loops and asterisks represent magnetic field sensors.

structure in close proximity to the plasma region is generally required in the reconstructions. Since the one-turn electrical resistance of vacuum vessel components increases linearly with major radius, the low aspect ratio NSTX vessel carries a greater induced current for a given applied transformer voltage compared to a conventional aspect ratio tokamak.

The NSTX vacuum vessel and conducting stabilizing plates are modeled as a collection of single-turn, parallel conductors. The vessel components are divided into 20 independent current carrying regions, and the combination of the passive conducting plates and divertor plates are divided into 10 regions. An effective resistance for each region is computed by fitting the vacuum field of NSTX with EFIT. The reconstructed currents in each vessel segment region are then compared to the voltage measured in a neighboring loop voltage sensor, yielding a resistance, $R_{eff,i} = V_{loop,i} / I_i$. The values computed by the fit, and the resulting current distribution in the vessel agree with equivalent eddy-current code calculations. The total computed current agrees with the value measured by the plasma current Rogowski coil within the stated error. The resistance vector is then used to compute the current for each vessel segment region, given the measured loop voltages, for subsequent reconstructions of the plasma equilibria. These currents are then fitted, along with the other magnetic measurements when computing the equilibrium solution. Since the discrete loop voltage sensors do not identically reproduce the voltage over the vessel segment region to which they are matched, the computed currents are input to the reconstruction with relatively large error bars (~ 20%). This error is small enough to prevent the algorithm from minimizing χ^2 at an unphysical solution, yet is large enough to permit the solution to deviate from the computed value during periods of fast current transients. Measurements of the currents in the passive conducting plates and the divertor plates are not yet available. Calculations using the SPARK code [6] of the 3-D eddy currents in these regions during an NSTX discharge indicate axisymmetric equivalent currents that flow in opposing directions in the top and bottom of a given plate. The magnitude of these currents is a few kA. The input to the reconstruction is therefore set at zero current for the plates, with an error of +/- 3kA to allow currents of this magnitude to flow in these regions. Typically, currents are reconstructed in these regions which may resemble the axisymmetric equivalent current pattern, but the present diagnostic set does not allow reliable reconstruction of these currents. NSTX will be instrumented with additional diagnostics to accurately determine the magnitude of these currents.

Another consideration for the equilibrium fitting is the choice of constraints for the basis function model. The integral relations obtained from the general MHD equilibrium equation generally lead to a solution for $\Lambda = \beta_p + \ell_i / 2$ [7]. However, for plasmas with sufficiently non-circular cross section, equation (4) of Ref. [7] can be used to separately determine β_p and ℓ_i from external magnetic measurements alone. These three equations indicate that three free parameters can be used to describe three global quantities for the equilibrium, typically, I_p, β_p, and ℓ_i.

For NSTX plasmas, a reliable basis function set for p' and ff' is

$$p'(\psi) = A_1 \psi_n (1 - \psi_n) \qquad (7)$$

$$ff'(\psi) = B_0 + B_1 \psi_n - (B_0 + B_1)\psi_n^2. \quad (8)$$

This model, which has three free parameters, constrains the toroidal plasma current at the edge to zero. This is satisfactory to reconstruct quasi-stationary NSTX plasmas, however, it fails to track large, fast transients in the current profile, including reconnection events that significantly alter ℓ_i. Note that this model employs the constraint that $p' = 0$ at the magnetic axis.

It is found that finite edge current density can be modeled reliably if one higher order is allowed in the ff' profile, and the constraints of $p' = 0$ on axis, and $(ff')' = 0$ at the plasma edge are imposed, the latter constraint allowing for finite edge current density. This model has four free parameters. Normally, allowing this extra degree of freedom requires imposing an additional constraint - for example, the safety factor at the magnetic axis, q_0. However, for NSTX, it is found that if the input magnetics have sufficient accuracy and are free of large discrepancies, the extra degree of freedom in ff' need not have an additional constraint imposed as long as the constraint of $p' = 0$ on axis is imposed.

Since measurements of the internal magnetic field are not yet available on NSTX, constraining q_0 is not justified. However, since sawteeth are observed in NSTX plasmas, the time evolution of q_0 can be compared to the appearance of sawteeth. Basis function models of lower order and with different constraints have been tried, and the model given above best correlates the temporal crossing of $q_0 = 1$ and the onset of sawteeth. This correlation is demonstrated in FIG. 2. For 80 plasmas examined, sawteeth appear when $q_0 = 0.96$ +/- 0.05.

The choice of basis function models and vessel current specification described above have sufficient freedom to reconstruct equilibrium quantities such as stored energy with small noise, yet can reproduce fast current perturbations. This prescription is used for between-shots analysis of NSTX plasmas, which typically produces 150 reconstructions per shot. While the reconstructions cannot always follow some of the larger transients, it is normal for all input magnetics signals to be reproduced within the stated error over the entire evolution of the plasma.

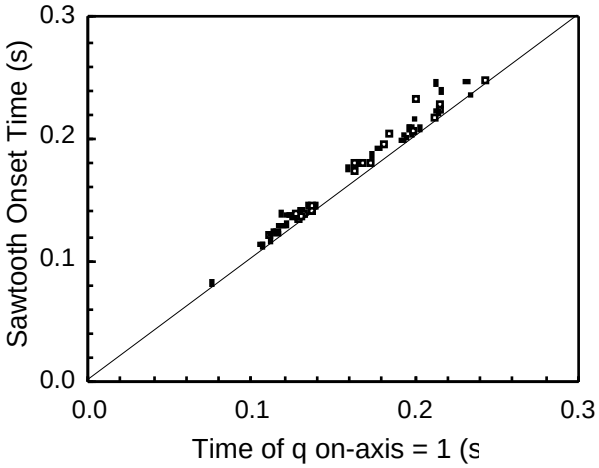

FIG. 2. Onset time of sawteeth in NSTX vs. time of $q_0 = 1$ crossing from discharge reconstructions.

3. Experimental results

3.1. Establishing plasma equilibria

Research in NSTX is being conducted to establish the equilibrium configurations to be used in high-β experiments with intense neutral beam and high-harmonic fast wave heating [8]. The device has a major radius, $R_0 = 0.86$ m, and a midplane half-width of 0.7 m. The machine has been operated with deuterium or helium gas, with an on-axis vacuum toroidal field, $B_0 \leq 0.3$ T and plasma current, $I_p \leq 1.1$ MA. Peak electron densities of 8×10^{19} m^{-3} have been produced in helium and 5.5×10^{19} m^{-3} in deuterium plasmas. Pulse lengths have been extended to 0.5s at $I_p \leq$ 0.5 MA. The plasma current, and radial and vertical position are controlled by real-time feedback of the poloidal field coil currents [9] while the plasma shape is presently controlled by pre-programming currents in the poloidal field shaping coils. To minimize impurity influx, the graphite tile surface facing the plasma was conditioned by a glow discharge in a mixture of trimethylboron and helium. Details of the plasma startup and flux consumption before and after the application of boron are given in Ref. [10].

The plasma boundary configurations and the operational space envisioned during the design phase of NSTX have been produced. Limiter, double-null, and lower single-null diverted

configurations (FIG. 3) have been created. Each configuration was sustained at a nominally constant I_p for a duration of several energy confinement times. These target plasmas have been successfully heated with up to 3 MW of high-harmonic fast wave (HHFW) power, [8] and separately with 2.8 MW of neutral beam power. In these cases, Wtot has reached 56 kJ (β_t = 10%; β_N = 2.8), and 92 kJ (β_t = 17.8%; β_N = 3.1), respectively, with energy confinement times at peak stored energy (not including shine through and other losses) of 15 ms and 20 ms.

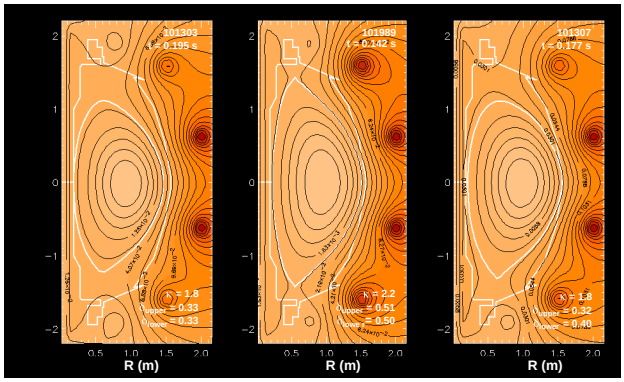

FIG. 3. Reconstructions of poloidal flux contours for limited, double-null, and lower single-null diverted equilibria.

FIG. 4 illustrates the evolution of plasma parameters for an ohmic, double-null diverted plasma with I_p = 0.7 MA. The configuration is maintained for 3 energy confinement times, τ_E. Plasma stored energy, W_{tot}, reaches 43 kJ, which equates to β_t = 7.8% at an ohmic input power of 1.1 MW at peak W_{tot}. The corresponding τ_E is 40 ms. Because of the reduced resistance of the low aspect ratio vessel components, the proximity of the conducting structure, and the appreciable loop voltage (2-6 V) used during the I_p increase, the induced currents flowing in the vacuum vessel wall and stabilizing conducting plates can be significant and are necessarily included in the reconstructions. The induced wall current, I_w, varies between 0.2 and 0.25 MA from the first reconstruction at t = 25 ms until peak I_p is reached. The largest W_{tot} in ohmic plasmas were attained with the highest values of plasma current, electron density, n_e, and plasma volume, V. These plasmas are paramagnetic, and due to the low aspect ratio and low toroidal field of the device, have large magnetic field pitch angle at the plasma edge in excess of 45 degrees at I_p = 1 MA.

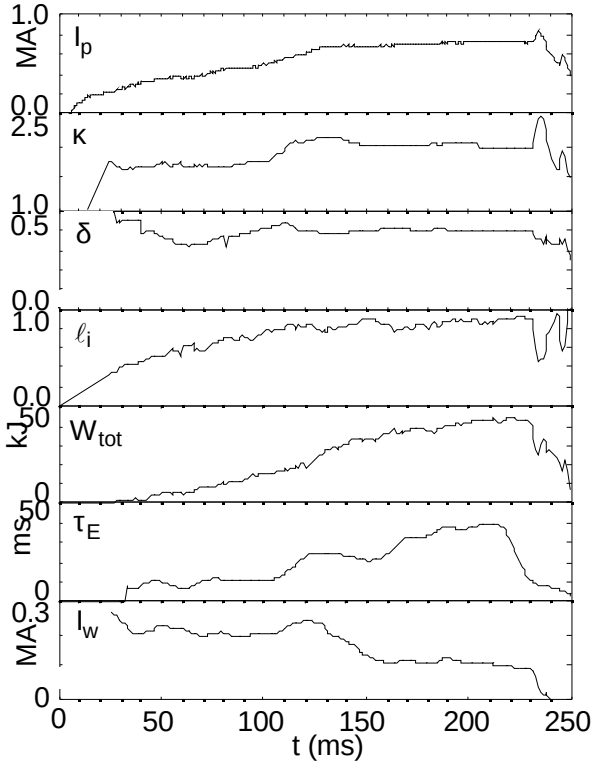

FIG. 4. Time evolution of EFIT reconstructed plasma parameters for an NSTX ohmic discharge. The interval between reconstructions is 1 ms.

Energy confinement time in both deuterium and helium ohmic plasmas exhibit trends that are similar to those at conventional aspect ratio (FIG. 5). For low to moderate densities ($\leq 4\times10^{19}$ m^{-3}, corresponding to $n_e/n_{e\,GW} \leq 0.8$), where the Greenwald density $n_{e\,GW} \equiv I_p/\pi a^2$, where a is the plasma minor radius, the energy confinement time in both species increases approximately linearly with line-averaged density to a value of 45 ms. Densities greater than 4×10^{19} m^{-3} were attained only in post-boronized helium plasmas, and for these the confinement time is seen to drop to values of about 20 ms at the highest density (5.5×10^{19} m^{-3}, corresponding to $n_e/n_{e\,GW} \sim 1.2$). At $n_e/n_{e\,GW}$ = 0.8, the maximum τ_E is approximately 1.4x $\tau_{E\,ITER89\text{-}P}$, while $\tau_E / \tau_{E\,ITER89\text{-}P}$ = 0.8-1.0 at the higher densities. For the ITER89P scaling in this case, the mass scaling parameter was taken to be M_{eff}/Z_{ion}, which is 2 for either species. The confinement time in the post-boronized plasmas was not necessarily greater than that in the pre-boronized plasmas at the same density; boronization, however, served to extend the accessible density range.

3.2. Plasma boundary and profiles

As discussed in Section 2.2, the equilibrium reconstructions fit well to the external magnetic measurements. The response of equilibrium parameters to plasma dynamics and perturbations are reproduced in detail as a function of time, including the general time evolution of q_0. In addition, aspects of the plasma boundary, pressure, and q profiles that define the plasma equilibria can be assessed using non-magnetic diagnostics. Evolution of the reconstructed plasma configuration agrees with visible light emission from the plasma imaged at 1 kHz. [11]

FIG. 6 shows a comparison of these results for events which illustrate the plasma boundary in the fast camera images. Early, small-bore plasma evolution, transition to a lower single-null diverted plasma, and the return of the plasma to the center stack limiter before

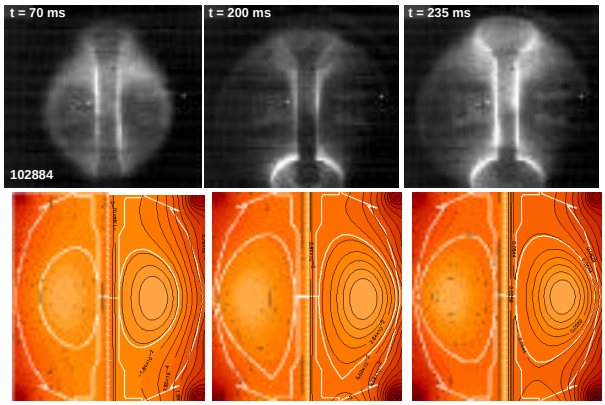

FIG. 6. Comparison of visible-light images of the evolution of the plasma boundary and magnetic reconstructions.

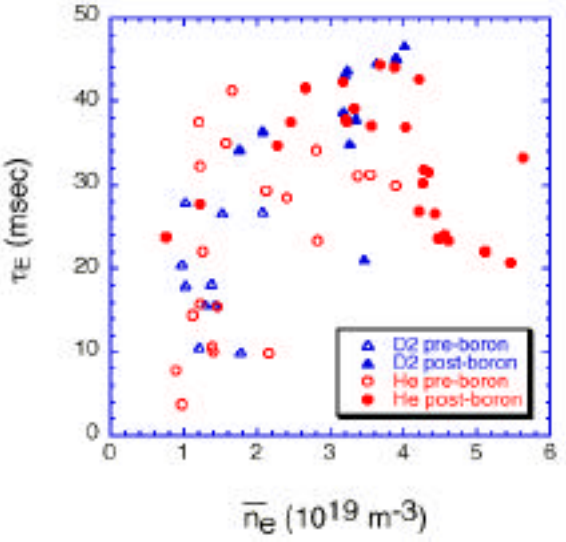

FIG. 5. Energy confinement vs. line-averaged density in deuterium and helium plasmas, pre- and post-boronization.

shutdown are compared to the boundary reconstructions from magnetics. The two bright points in each frame are tungsten filaments. In the first frame, the plasma boundary is in the field of view of the camera. In the remaining frames the boundary at large major radius is outside the field of view. In the second frame, the dark center column, visible scrapeoff region, and bright lower divertor region indicate a lower single null plasma with a small inner gap. The final frame shows the plasma moving back to the center column limiter which becomes bright with a small dark band near the lower portion of the column. These features are all consistent with the details of the reconstructed plasma boundary shape.

The multi-pulse Thomson scattering diagnostic yields a time evolution of the electron pressure profile. The stored energy in the electrons is typically 40 - 50% of the total stored energy in ohmic plasmas, as high as 70% in HHFW plasmas, and greater than 25% in plasmas heated with neutral beams. Note that the present Thomson scattering data are based on Rayleigh calibration. Preliminary examination of reflectometer data suggest somewhat lower density. The magnetic axis position of the electron pressure profile agrees well with the equilibrium analysis. FIG. 7 shows the time evolution of the reconstructed magnetic axis and that given by the electron pressure profile. Note that the latter is determined by a spline fit of the pressure using channels that are separated by about 15 cm, so uncertainty of several centimeters is not unexpected. The two measurements are in agreement through the large reconnection event at $t = 0.27$ s. The discrepancy at the initial time point shown is due to the electron pressure profile being hollow, and the EFIT reconstruction being less reliable since the plasma current is about equal to the current in the vacuum vessel wall at this early time.

In addition to the q_0 evolution being consistent with the onset of sawteeth (FIG. 2), the position of the inversion radius of the soft X-ray signals gives an indication of the radial position of the $q = 1$ surface. FIG. 8 shows good agreement between the radial positions of the EFIT $q = 1$ surface and the inversion radius from an inversion of 45 soft X-ray chords. The plasma has a

large q = 1 region, consistent with the observation of a large sawtooth amplitude in this discharge. Operational limits associated with the large sawteeth in this plasma are discussed in the next section.

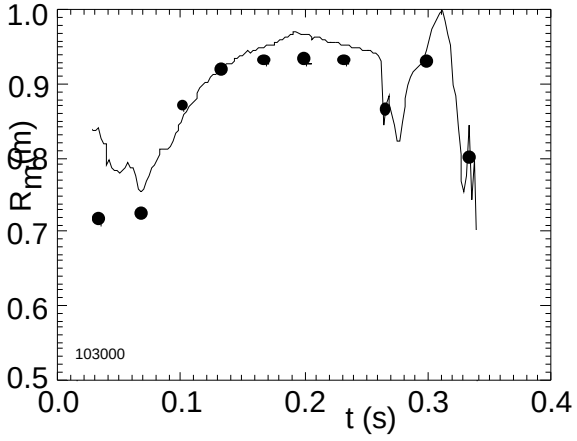

FIG. 7. Comparison of reconstructed magnetic axis position (curve) and axis position from multi-pulse Thomson scattering diagnostic (points).

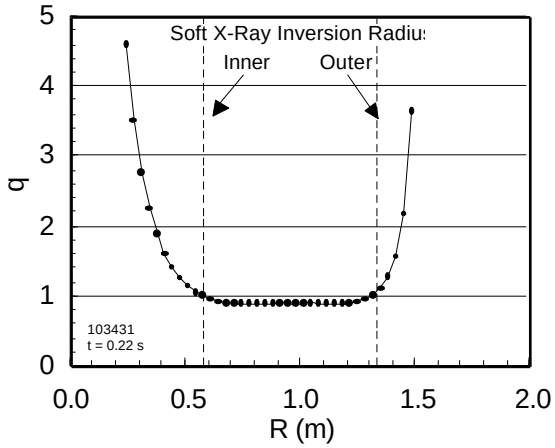

FIG. 8. EFIT q profile versus major radius and position of soft X-ray inversion radius.

3.3. Operational space and instabilities

A primary objective in establishing the first equilibria in NSTX was to determine the range of boundary shapes possible in the experiment. Plasma elongation of $1.6 \le \kappa \le 2.0$ and triangularity in the range $0.25 \le \delta \le 0.45$ have been sustained, while maximum values of $\kappa = 2.5$ and $\delta = 0.6$ have been reached transiently. A subset of the present NSTX database of (κ,δ) is shown in FIG. 9.

Density limits in NSTX ohmic plasmas were explored in both deuterium and helium by varying the gas puff rates from discharge to discharge. These experiments were conducted in pre- and post-boronized plasmas for both species. FIG. 10 shows the achieved line-averaged electron density as a function of $n_{e\,GW}$. As can be seen, the pre-boronized plasmas attain densities up to only 0.5 $n_{e\,GW}$, for either deuterium or helium. After the first boronization, the achievable densities were considerably higher, with deuterium plasmas reaching $n_e = 0.8\ n_{e\,GW}$ (4×10^{19} m^{-3}) and helium reaching $1.2\ n_{e\,GW}$ (5.5×10^{19} m^{-3}). Also shown in the plot are two points from RF heated discharges where $n_e/n_{e\,GW}$ =1.2, but in these cases, the RF power was less than 20% of the ohmic heating power.

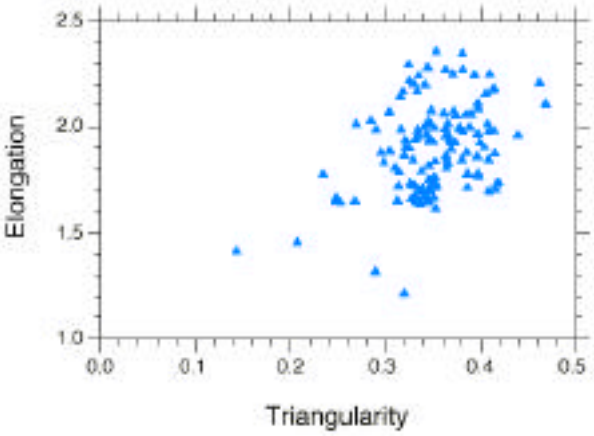

FIG. 9. Operational space of NSTX boundary parameters at peak stored energy.

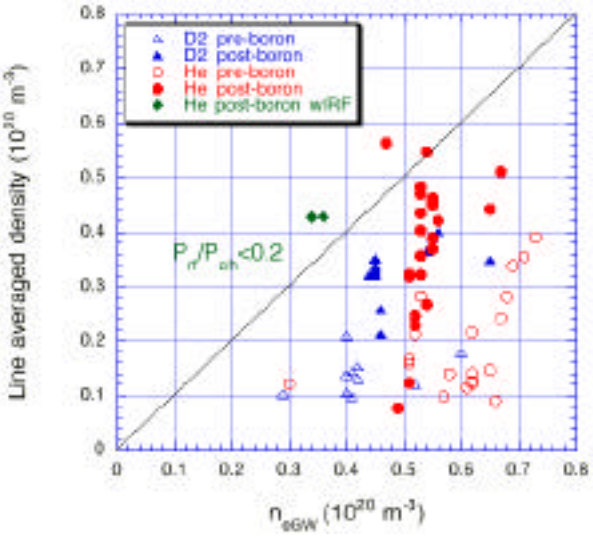

FIG. 10. Line-averaged electron density versus Greenwald density in deuterium and helium plasmas, pre- and post-boronization.

One major difference between deuterium and helium plasmas at higher density was the amount of Carbon-III light, which was much greater in deuterium plasmas presumably due to chemical sputtering of the graphite tiles. For both species, in both the pre- and post-boronized plasmas, the radiated power was typically ≤ 30% of the ohmic heating power at the time of maximum density. The only MHD observed at the time of the density limit in the highest density cases was sawteeth, and investigations are underway to determine whether the limit is related to the sawteeth, or whether fueling limitations set the maximum density.

Instabilities characterized as reconnection events (REs), both internal and global, in previous ST experiments [12] have been observed in NSTX during both the increase and reduction of the plasma current. These events are evidenced by Mirnov oscillations, spikes in the I_p evolution, D_α and Carbon-III light,and when sufficiently large, alteration of the plasma internal inductance and elongation. For events close to the end of the pulse (leading to, or during the ramping-down of I_p) a large, transient decrease of ℓ_i (of up to 50%) can occur, with a simultaneous increase in the elongation. Animation of the poloidal flux contours show that both the boundary and the inner flux surfaces elongate in a similar fashion. A low q limit was encountered at a $q_{cyl} = 2.5a^2B_t(1 + \kappa^2)/RI_p \approx 1.4$ by ramping down B_t at constant plasma current. The limit is manifest by a low toroidal mode number kink instability that terminates the discharge. The low-n, non-axisymmetric nature of the mode is apparent from 1 kHz sampled visible-light images of the plasma. At the onset of instability, β_t and β_N were 9% and 1.7, respectively at $B_0 = 0.18$ T.

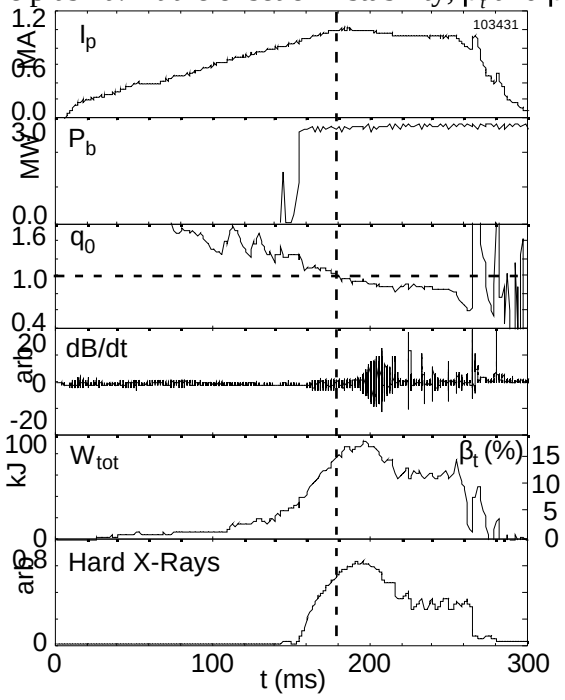

FIG. 11. Onset of 1/1 mode and subsequent large sawtooth oscillation in a high β *plasma.*

A global beta limit has not yet been conclusively reached in NSTX. Fast termination of discharges at relatively high beta has been observed in neutral beam heated discharges with a large rate of rise in the plasma stored energy (dW_{tot}/dt = 1.3 - 2 MW). The termination occurs for a wide range of β_t ~ 10 - 18%, below the values expected for an ideal global kink/ballooning mode. In these plasmas, q_0 drops below unity without a stable sawtooth oscillation. The termination appears to be due to a large reconnection event that would normally be a less perturbative sawtooth oscillation observed in plasmas with less aggressive heating.

The sawtooth oscillation in high beta plasmas can also lead to a saturation and rollover of the plasma stored energy. This is illustrated in FIG. 11. Approximately 20 ms after the start of 2.7 MW of NBI heating, the q_0 is observed to cross below unity. At this time, a small m/n = 1/1 mode commences and continues to grow. The peak W_{tot} is reached as the oscillation increases in magnitude, and finally the plasma suffers a large sawtooth crash. The change in W_{tot} is 15 kJ during the first cycle, which is 20% of the stored energy before the crash. The magnitude of the oscillation is evident in the W_{tot} waveform until the terminating RE occurs. The detail of the evolution of W_{tot} is identical to the evolution of the hard X-ray detector (an indicator of neutron production) during this period of time.

4. Ideal Stability Limits

With equilibrium profiles optimized for ideal MHD stability, NSTX can theoretically reach β_t in excess of 40% [13]. Studies utilizing profiles from neutral beam heated tokamak and ST experiments show that while these high β targets are possible, a limit to either high-n ballooning

or low-*n* kink/ballooning modes might be observed at significantly lower values between 20 - 25% [14].

Auxiliary heated NSTX plasmas that have reached β_N = 2.8 - 3.1 have been used to determine the ideal stability limit by fixing the plasma boundary and scaling the pressure profile self-similarly. The DCON [15] and GATO [16] ideal stability codes were used to compute the low-*n* stability for these high β equilibria with q_0 = 1.2. The extrapolated equilibrium is unstable at β_N = 4.7 in a double-null configuration and β_N = 4.5 in a single null configuration to a global kink/ballooning mode. This mode has a strong internal component, so for these particular equilibria, the stabilizing conducting plates do not significantly alter the beta limit. Future NSTX research will include testing computed stability limits, and determination of the scaling of these limits based on global as well as profile parameters.

Acknowledgements

Jon Menard is especially acknowledged for performing the difficult task of providing highly accurate magnetics data essential to this analysis. This research was supported by the U.S. Department of Energy under contracts DE-FG02-99ER54524 and DE-AC02-76CH03073.

---

*Supported by US DOE Contracts DE-FG02-99ER54524 and DE-AC02-76CH03073.

[1] STAMBAUGH, R.D., CHAN, V.S., MILLER, R.L. *et al., Fusion Technology* **33** (1998) 1.
[2] SYKES, A. *et al., Plasma Phys. Contr. Nucl. Fus. Res.* **1** (1994) 719.
[3] DARKE, A.C. *et al., Fusion Technol.* **1** (1995) 799.
[4] ONO, M. *et al., Phys. Plasmas* **4** (1997) 1953.
[5] LAO, L. L. *et al., Nucl. Fusion* **25** (1985) 1611.
[6] WEISSENBURGER, D.W. *et al.,* SPARK Version 1.1 User Manual, January 1988, Princeton Plasma Physics Laboratory Report PPPL-2494.
[7] LAO, L. L. *et al., Nucl. Fusion* **25** (1985) 1421.
[8] WILSON, R. *et al., "High Harmonic Fast Wave Heating Experiments on NSTX"*, presented at the 18th IAEA Fusion Energy Conference, Sorrento, Italy, 2000.
[9] GATES, D., MUELLER, D., NEUMEYER, C., and FERRON, J., *"Control System Development Plan for the National Spherical Torus Experiment", Proceedings of the Eleventh IEEE NPSS Real Time Conference*, 1999, S. Schaller, Editor.
[10] MENARD, J. *et al., "Ohmic Flux Consumption During Initial Operation of NSTX"*, presented at the 18th IAEA Fusion Energy Conference, Sorrento, Italy, 2000; submitted to *Nucl. Fusion.*
[11] MAQUEDA, R. and WURDEN, G., *Nucl. Fusion* **39** (1999) 629.
[12] SYKES, A. *et al., Nucl. Fusion* **32** (1992) 694.
[13] MENARD, J. *et al., Nucl. Fusion* **37** (1997) 595.
[14] PAOLETTI, F., SABBAGH, S.A., GATES, D., *et al., "Impact of Profile Variation on the Equilibrium and Stability of NSTX", Proc. 25th EPS Conf. On Contr. Fusion and Plasma Physics, Maastricht* **23** (1999) 1709.
[15] GLASSER, A.H., *"The Direct Criterion of Newcomb for the Stability of an Axisymmetric Toroidal Plasma".*
[16] BERNARD, L. C., HELTON, F. J., MOORE, R. W., *Comp. Phys. Communications* **24** (1981) 377-380.